Journal of Environmental Radioactivity 247 (2022) 106864

Contents lists available at ScienceDirect

Journal of Environmental Radioactivity

journal homepage: www.elsevier.com/locate/jenvrad

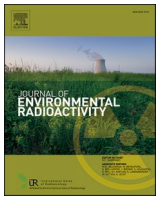

Zonal and vertical transports of Fukushima-derived radiocesium in the subarctic gyre of the North Pacific until 2014

Yuichiro Kumamoto [a,*], Michio Aoyama [b], Yasunori Hamajima [c], Hisao Nagai [d], Takeyasu Yamagata [d], Akihiko Murata [a]

[a] Research Institute for Global Change, Japan Agency for Marine-Earth Science and Technology, 2-15 Natushima-cho, Yokosuka, Kanagawa, 237-0061, Japan
[b] Center for Research in Isotopes and Environmental Dynamics, University of Tsukuba, 1-1-1 Tennodai, Tsukuba, Ibaraki, 305-8577, Japan
[c] Low Level Radioactivity Laboratory, Kanazawa University, Wake, Nomi, Ishikawa, 923-1224, Japan
[d] Department of Chemistry, College of Humanities and Sciences, Nihon University, 2-25-40 Sakura-josui, Setagaya, Tokyo, 156-8550, Japan

ARTICLE INFO

Keywords:
Nuclear power plant accident
Ocean tracer
Kuroshio extension current
North pacific current
Mode waters

ABSTRACT

The Fukushima Dai-ichi Nuclear Power Plant (FNPP1) accident in March 2011 resulted in serious radiocesium contamination of the North Pacific Ocean. Most of the radiocesium was dissolved in seawater and transported by surface currents and subduction of mode waters. Within several years after the accident, a high-concentration water plume of the FNPP1-derived radiocesium at the sea surface had been transported from Japan to the North American continent across the subarctic gyre of the North Pacific Ocean. We measured vertical profiles of dissolved radiocesium along the nominal 47°N zonal line across the North Pacific subarctic gyre twice, in summer 2012 and summer 2014. Using these data and published data, we quantitatively discussed the zonal and vertical transports of the water plume until 2014. The FNPP1-derived radiocesium remained in the surface layer shallower than 200 m, which is the approximate winter mixed-layer depth in the western subarctic gyre. The mean penetration depth did not change between 2012 and 2014. The highest concentration was observed at 180°W in 2012 and at 151°W in 2014, which suggests that the zonal transport speed of the water plume in the eastern subarctic gyre was about 3.8 cm s^{-1}. By combining the data from the zonal line in 2014 and a nominal 152°W meridional line in 2015, we elucidated the three-dimensional size of the high-concentration water plume in summer 2014. The total inventory of the FNPP1-derived radiocesium in the subarctic North Pacific Ocean, decay-corrected to the accident date, was estimated to be 12.0 ± 2.4 PBq.

1. Introduction

The massive earthquake in the North Pacific Ocean off northeast Japan and the giant tsunami on 11 March 2011 resulted in serious damage to the Fukushima Dai-ichi Nuclear Power Plant (FNPP1) because of its location (37.4°N/141.0°E) on the North Pacific coast of Japan (Fig. 1). Consequently, radiocesium (^{134}Cs and ^{137}Cs) and other radionuclides were released from the damaged FNPP1 to the environment (Buesseler et al., 2011). Just after the accident, a major portion of the radiocesium released to the atmosphere was carried eastward by the prevailing westerly winds and deposited across a broad region of the northern North Pacific Ocean north of 30°N approximately (the yellow and light-yellow shadows in Fig. 2a; Buesseler et al., 2017). Subsequently, in late March 2011, radioactive water containing radiocesium from the FNPP1 was discharged directly to the ocean (the red shadow in Fig. 2a; Buesseler et al., 2017). Estimates of spreading process and the total input of FNPP1-derived radiocesium in the North Pacific Ocean are essential for studies of marine environmental radioactivity. However, quantitative discussion of the FNPP1-derived radiocesium in the ocean has been more difficult than that deposited on land (e.g. Morino et al., 2013), because the oceanic radiocesium was immediately dissolved in seawater, diluted by water mixing, and transported by water advection, unlike the onshore radiocesium.

The total release activities of ^{134}Cs and ^{137}Cs from the FNPP1 were equivalent (Buesseler et al., 2017). Before the FNPP1 accident, ^{137}Cs had been also released into the North Pacific Ocean mainly by atmospheric testing of nuclear weapons in the 1950s and 1960s. This bomb-derived ^{137}Cs in the North Pacific remained just before the FNPP1 accident

* Corresponding author. .
E-mail addresses: kumamoto@jamstec.go.jp (Y. Kumamoto), michio.aoyama@ied.tsukuba.ac.jp (M. Aoyama), hamajima@se.kanazawa-u.ac.jp (Y. Hamajima), hnagai@chs.nihon-u.ac.jp (H. Nagai), yamagata@chs.nihon-u.ac.jp (T. Yamagata), murataa@jamstec.go.jp (A. Murata).

https://doi.org/10.1016/j.jenvrad.2022.106864
Received 26 June 2021; Received in revised form 6 March 2022; Accepted 8 March 2022

because of its long half-life (30.04 y), which is estimated to be 69 PBq (10^{15} Bq) (Aoyama et al., 2016a). In contrast, virtually all of the ^{134}Cs released into the North Pacific before the FNPP1 accident had disappeared, because of its negligible input from the nuclear weapons testing and short half-life (2.07 y). Therefore, ^{134}Cs is potentially more suitable than ^{137}Cs for tracing FNPP1-derived radiocesium. In the remainder of this paper, we discuss only activity concentration and inventory of ^{134}Cs decay-corrected to the date of the FNPP1 accident (11 March 2011), which are equivalent to those of FNPP1-derived ^{137}Cs, respectively.

Estimates of the total atmospheric release of ^{134}Cs range widely from 9 to 50 PBq, because there is paucity of observational data from the vast North Pacific that are required to conduct inverse calculations in atmospheric models (Buesseler et al., 2017). As a result, estimates of the atmospheric-deposited ^{134}Cs on the North Pacific also range widely. In 2016, a more accurate estimate of 12–15 PBq in the North Pacific was derived by means of a detailed tally of field-based inventories across the basin in April–June 2011, just after the FNPP1 accident (Aoyama et al., 2016a). Estimates of the subsequent direct discharge of ^{134}Cs also vary greatly, from 3 to 27 PBq (Buesseler et al., 2017), although the larger values may be overestimates due to inadequate time series back-calculations (Tsumune et al., 2013). At present, estimates of the total ^{134}Cs input from the FNPP1 accident into the North Pacific tend to converge on a range of 15–20 PBq (Buesseler et al., 2017), 12–15 PBq of which was deposited from the atmosphere (the yellow and light-yellow shadows in Figs. 2a) and 3−5 PBq of which was directly discharged into the ocean (the red shadow in Fig. 2a). The equivalent release of FNPP1-derived ^{137}Cs (15–20 PBq) corresponds to an increase of about 20–30% compared with the inventory of ^{137}Cs in the North Pacific before the FNPP1 accident, 69 PBq (Aoyama et al., 2016a).

The ^{134}Cs atmospheric-deposited and directly-discharged has spread at the surface of the North Pacific Ocean along with the two basin-scale surface circulations, the anti-clockwise subarctic and clockwise subtropical gyre circulations (Fig. 1). In the mid-latitude around 30−45°N between the two circulations, there are strong eastward currents (the Kuroshio Extension and North Pacific Currents). In April 2011, about one month after the accident, ^{134}Cs was detected at the sea surface west of 46°N/162°W, about 4700 km away from the FNPP1 (Fig. 2a; Aoyama et al., 2013). This ^{134}Cs measured at the long-distance station within one month after the accident was probably transported by atmospheric deposition, not by surface seawater currents. Then, it was subsequently transported further eastward along with the subarctic gyre circulation and arrived at Station P (50°N/145°W), a time-series observational station, in June 2012 (Fig. 1), and at 49°N/127°W in June 2013 (Smith et al., 2015).

Following the ^{134}Cs widely atmospheric-deposited over the North Pacific, a plume of high-^{134}Cs concentration water at the sea surface, which originated from both atmospheric deposition near the FNPP1 and direct discharge from the FNPP1 (the yellow and red shadows in Fig. 2a), was also transported eastward (Aoyama et al., 2016b; Kaeriyama et al., 2013; Smith et al., 2017). Because the FNPP1 locates just north of the Kuroshio Extension Current or Front (Fig. 1), the water plume was transported eastward in the southern area of the subarctic gyre. Specifically, a plume of water with a high ^{134}Cs concentration of more than 4 Bq m^{-3} was observed around 35−40°N/145−155°E in June−August 2011 (Kumamoto et al., 2014), 38−48°N/160°E−170°W in August−December 2012 (Kumamoto et al., 2016), and 32−54°N/160−130°W in June−August 2015 (Smith et al., 2017). At Station P, ^{134}Cs concentration had increased due to the arrival of this plume by February 2014 (the orange shadow in Fig. 2b; Smith et al., 2015), about two years after the arrival of the atmospheric-deposited ^{134}Cs by June 2012. Then the water plume had arrived at the North American continent by 2016 (Smith et al., 2017).

The vertical transport of FNPP1-derived ^{134}Cs into the ocean interior was derived from vertical mixing at the sea surface. The deepest vertical mixing, the maximum of which is 400 m approximately, occurs in the mid-latitude around 30−45°N in the western North Pacific in the mid-winter (February and March). The surface mixed-layer water is then conveyed southward through the subsurface isopycnic layers below the local surface mixed-layer in the south. This southward-advecting subsurface water is called “mode water” and a few mode waters have been found in the western North Pacific Ocean (Oka and Qiu, 2012). In March/April 2011, just after the FNPP1 accident, the subtropical mode water (STMW; Masuzawa, 1969) and central mode water (CMW; Suga et al., 1997) were formed in areas south and north of the Kuroshio Front (the green and blue shadows in Fig. 2a) and started to subduct southward. As a result, a portion of ^{134}Cs in the offshore area of the FNPP1 was transported southward in the subsurface layers along with the

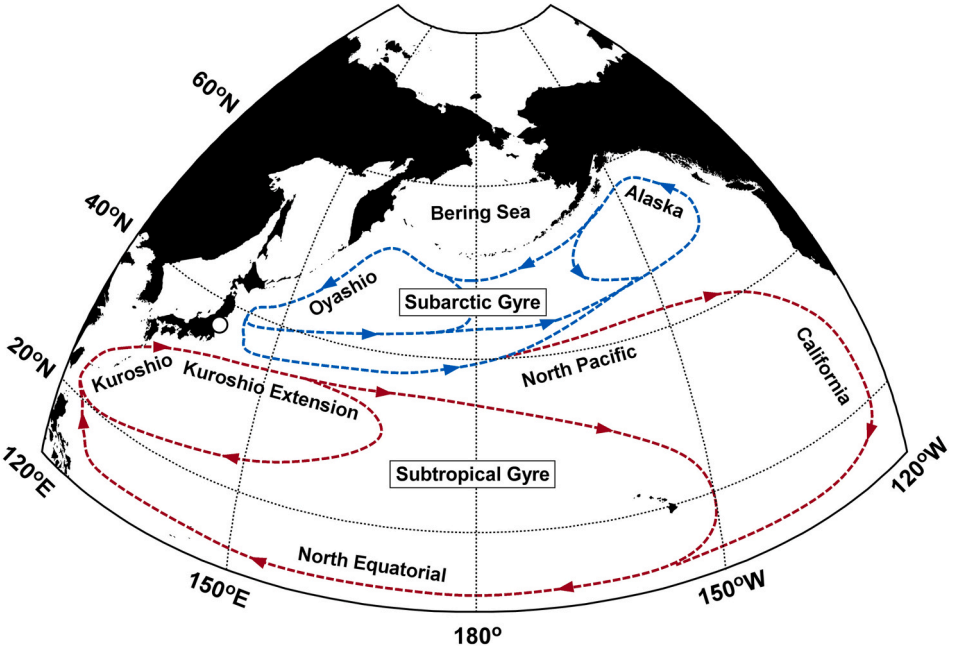

Fig. 1. Rough schematic view of basin-scale surface currents in the North Pacific Ocean. The white circle indicates the FNPP1 (37.4°N/141.0°E).

subduction of the mode waters while a larger portion of them was transported eastward in the surface layer along with the surface currents (Fig. 2b). Measurements of ^{134}Cs vertical profiles in the western North Pacific (Aoyama et al., 2016b; Kaeriyama et al., 2014, 2016; Kumamoto et al., 2014, 2015, 2017a; Yoshida et al., 2015) have revealed ^{134}Cs subsurface maxima between 200 and 400 m depth in the western subtropical gyre, which corresponds to the STMW layer (the green shadow in Fig. 2b).

Inventory of ^{134}Cs was also estimated using the observational data in the open ocean without model simulations. The inventory in the subsurface STMW in the western subtropical gyre was estimated to be 3–6 PBq (Kaeriyama et al., 2016; Kumamoto et al., 2014). Macdonald et al. (2020) observed vertical distributions of ^{134}Cs along the 152°W meridional line between 3°N and 56°N in summer 2015. They found ^{134}Cs in the surface layer shallower than 400 m depth approximately north of 30°N and higher concentrations than 7 Bq m^{-3} at the sea surface between 41°N and 43°N. This ^{134}Cs observed in the surface layer probably corresponds to the high-^{134}Cs water plume originated from both atmospheric deposition near the FNPP1 and direct discharge from the FNPP1 (the orange shadow in Fig. 2b). They also estimated the inventory in the surface layer in the subarctic gyre north of 30°N to be 11–16 PBq in 2015 only using their data along the 152°W meridional line. The sum (14–22 PBq) of the subarctic (11–16 PBq) and subtropical (3–6 PBq) inventories, which was estimated only with the observational data, agrees with the total input into the North Pacific, 15–20 PBq (Buesseler et al., 2017), which was estimated with outputs of model simulations.

The basin-scale time evolution of the Fukushima-derived ^{134}Cs in the North Pacific reviewed above (Fig. 2) were derived from model simulations (Rossi et al., 2013; Rypina et al., 2014; Tsubono et al., 2016) and cross-basin observations of ^{134}Cs vertical profiles. The vertical profiles at stations along several meridional lines between 137°E and 152°W had

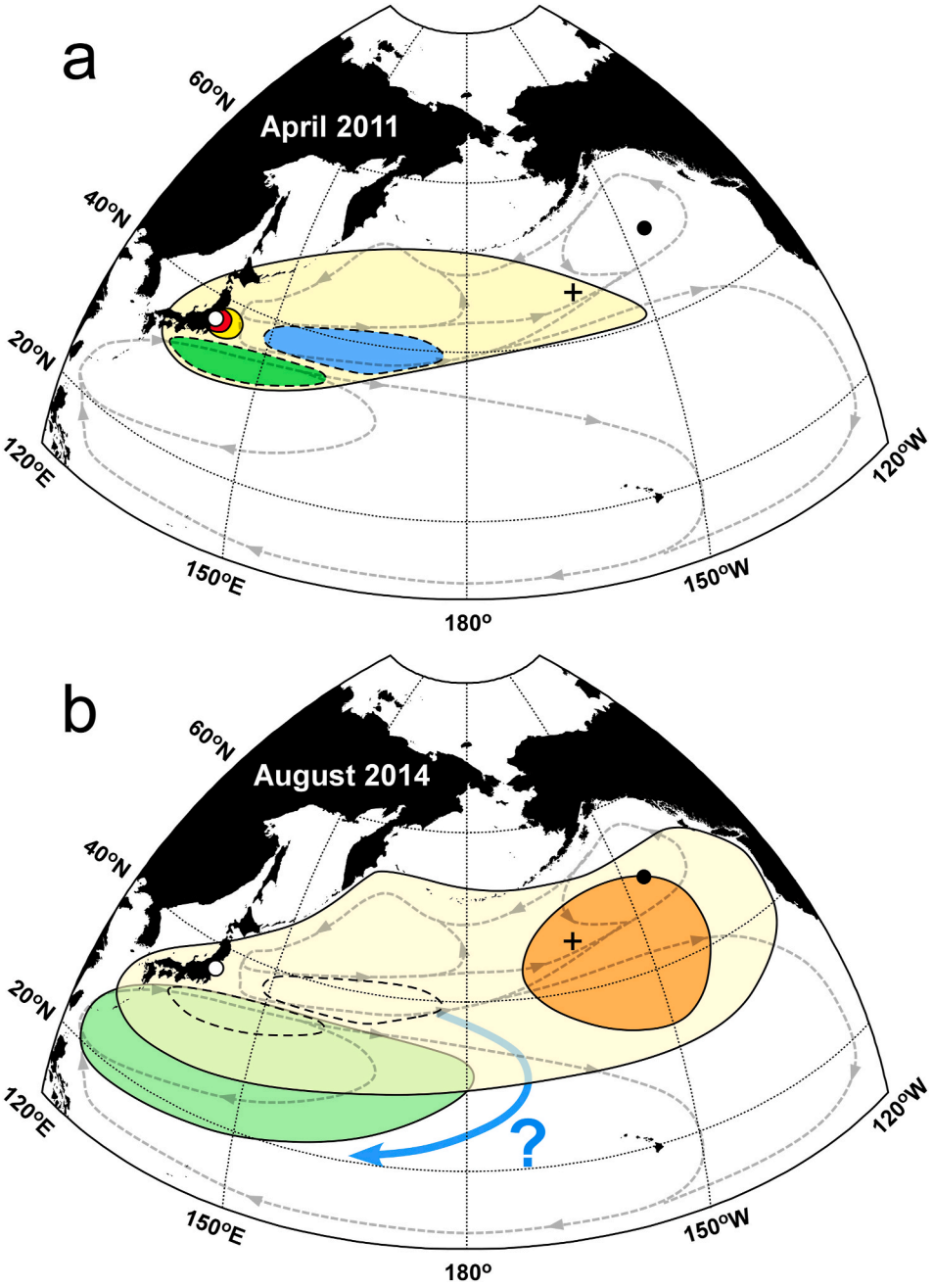

Fig. 2. (a) Schematic view of the distribution of FNPP1-derived ^{134}Cs at the sea surface in April 2011. The red, light-yellow, and yellow shadows indicate ^{134}Cs derived from the direct discharge, atmospheric deposition, and atmospheric deposition in the coastal area, respectively. The green and blue shadows are the formation areas of STMW and CMW, respectively. The white circle, black one, and cross indicate sites of the FNPP1 (37.4°N/141.0°E), Station P (50.0°N/145.0°W), and a sampling station (46.2°N/162.1°W) respectively. Broken arrows indicate surface currents. (b) Same as (a) but in August 2014. The orange shadow indicates the ^{134}Cs derived from the direct discharge and atmospheric deposition in the coastal area. The light-yellow shadow shows the ^{134}Cs derived mainly from the atmospheric deposition. The green shadow indicates the southward spreading of the atmospheric-deposited ^{134}Cs in a subsurface layer due to the subduction of STMW. The southward transport due to the subduction of CMW in a subsurface layer, which is deeper than that of STMW, has not been observed yet (the blue arrow). (For interpretation of the references to colour in this figure legend, the reader is referred to the Web version of this article.)

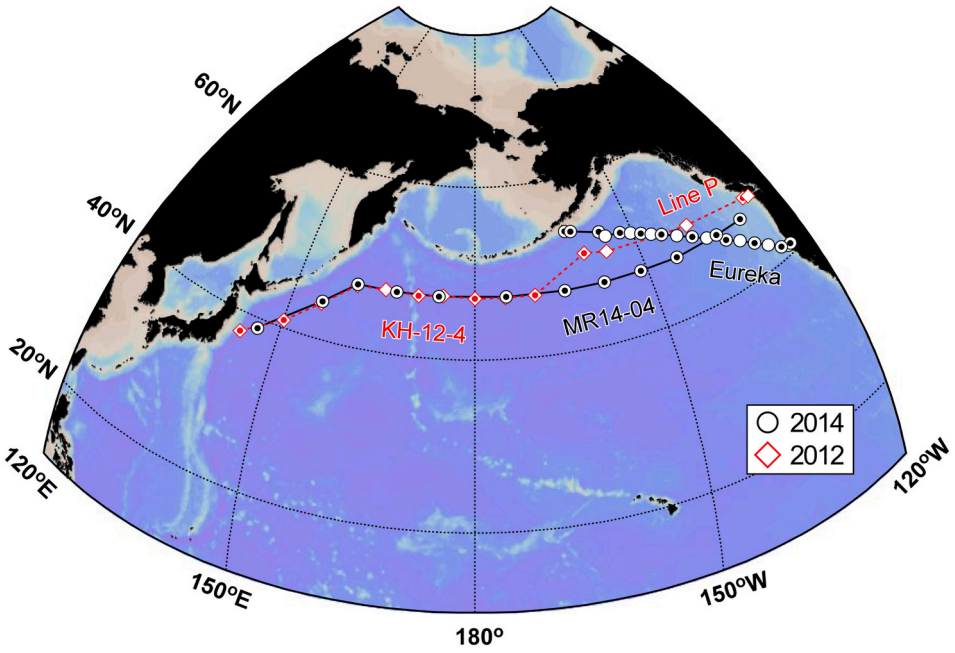

Fig. 3. Sites of the sampling stations for radiocesium measurements in 2012 (diamonds) and 2014 (circles) reported in this study. Circles with a center dot indicate stations that include the vertical profile.

been observed by 2015 (Aoyama et al., 2016b; Kaeriyama et al., 2014, 2016; Kumamoto et al., 2014, 2015, 2017a; Macdonald et al., 2020). On the other hand, a zonal observation across the North Pacific was conducted only once nominally along 30°N in the subtropical gyre in 2013 (Yoshida et al., 2015). In the Gulf of Alaska in the eastern subarctic gyre, the vertical profiles along Line P and Eureka line (Fig. 3) were measured between 2012 and 2016 (Smith et al., 2015, 2017; Yoshida et al., 2015). These elucidated the zonal and vertical transports of the Fukushima-derived ^{134}Cs in the Gulf of Alaska but not in the western and central areas of the subarctic gyre. Inomata et al. (2018) reported the vertical profiles at five stations nominally along 47°N between 150°E to 170°W in summer 2012. They, however, did not discuss the zonal distribution of the vertical profiles. As a result, zonal and vertical transport processes of the high-concentration water plume in the North Pacific subarctic gyre (the orange shadow in Fig. 2b) have not been achieved yet, although a larger portion of the Fukushima-derived ^{134}Cs had remained in the subarctic gyre until 2016.

In this study, we measured vertical profiles of dissolved radiocesium (^{134}Cs and ^{137}Cs) at stations along the nominal 47°N zonal line in the subarctic gyre in summer 2012 and summer 2014 (Fig. 3). Using these ^{134}Cs data and published data, we elucidated the zonal and vertical transports of the ^{134}Cs high-concentration water plume (the orange shadow in Fig. 2b) in the subarctic gyre until 2014. Furthermore, to achieve a three-dimensional size of the high-concentration water plume, we combined the zonal distribution along 47°N in 2014 with the meridional distribution along 152°W in 2015 (Macdonald et al., 2020). From these zonal and meridional cross-sections, we obtained a more robust inventory of ^{134}Cs in the subarctic gyre of the North Pacific than those estimated in the previous works (Inomata et al., 2018; Macdonald et al., 2020).

2. Methods and data

2.1. MR14-04-Leg2 cruise in summer 2014

During the MR14-04-Leg2 (L2) cruise in July–August 2014, we collected seawater samples at stations along the nominal 47°N zonal line (Fig. 3). This is a repeat hydrographic observation along the World Ocean Circulation Experiment (WOCE) P01 zonal line (expedition code: 49NZ20140717), and the hydrographic data are available on the CLIVAR (Climate Variability and Predictability) & Carbon Hydrographic Data Office (CCHDO) web page (CCHDO, 2021). Seawater samples (40 L) were collected from approximately 25 m–800 m depth by a carousel sampler equipped with 12-L plastic bottles and sensors for pressure, temperature, and conductivity, or from the surface with a bucket. Seawater samples from depths shallower than 100 m were filtered through a 0.45-mm pore size membrane filter on board, and salinity was measured with a salinometer. Dissolved radiocesium in the seawater sample was extracted and concentrated by using ammonium phosphomolybdate (AMP) (Aoyama and Hirose, 2008). The recovery of radiocesium by the AMP was about 92%. Radiocesium in the AMP was measured by using gamma-ray spectrometers at the Japan Agency for Marine-Earth Science and Technology or Kanazawa University. Detector efficiencies were measured by using the Deutscher Kalibrierdienst (DKD) calibration standards and the IAEA-443 Irish seawater reference material (Pham et al., 2011). The uncertainty and detection limit of ^{134}Cs (^{137}Cs) were about 18% (6%) and 0.5 (0.05) Bq m^{-3}, respectively. All radiocesium data from the MR14-04-L2 cruise (110 data) are listed in Table S1.

2.2. KH-12-4 cruise in summer 2012

Radiocesium data at five stations (48 data) among all data (105 data) of the KH-12-4 cruise have been published in our previous work (Inomata et al., 2018). However, because the sampling and analytical methods were not described, we note them hereinbelow. In August–September 2012 during the cruise, we collected seawater samples at stations along the nominal 47°N zonal line (Fig. 3). Seawater samples (20 L) were collected by using a large-volume sampler with four 250-L plastic bottles and pressure/temperature sensors from approximately 20 m–1000 m depth, or by an underway pump at about 5 m depth for surface water. Each sample was filtered through a 0.5-μm pore size wind-cartridge filter. Salinity of each sample was measured with a salinometer. Dissolved radiocesium in the seawater sample was extracted and concentrated on board by using AMP (Aoyama and Hirose, 2008). The recovery of radiocesium by the AMP was about 95%. Then, radiocesium in the AMP was measured by using gamma-ray spectrometers at Nihon University. Detector efficiencies were also measured by

using the DKD standards and the IAEA-443 reference (Pham et al., 2011). The uncertainty and detection limit of the ^{134}Cs (^{137}Cs) measurements were about 15% (8%) and 0.2 (0.05) Bq m^{-3}, respectively. All radiocesium data from the KH-12-4 cruise, including the published data in Inomata et al. (2018), are listed in Table S2.

2.3. Other data

To delineate the distribution of the ^{134}Cs activity concentration at the sea surface, we compiled datasets of ^{134}Cs measured in the North Pacific and its marginal seas in the summers of 2012 and 2014. The dataset from August–December 2012, except those from the KH-12-4 cruise (Table S2), have been published in our previous work (Inomata et al., 2018). The dataset from June–December 2014 (Aoyama et al., 2017; Inoue et al., 2016, 2018; Japan Nuclear Regulation Authority, 2021; Kumamoto et al., 2017a, 2017b; Smith et al., 2017; Yoshida et al., 2015), except those from the MR14-04-L2 cruise (Table S1), are listed in Table S3. We also utilized ^{134}Cs data along the nominal 152°W line measured in April–June 2015 (Macdonald et al., 2020). This is one of cruises conducted on the WOCE P16N repeat hydrographic line. Hydrographic data, including radiocesium concentration, of this cruise (expedition code: 33RO20150525 and 33RO20150410) are also

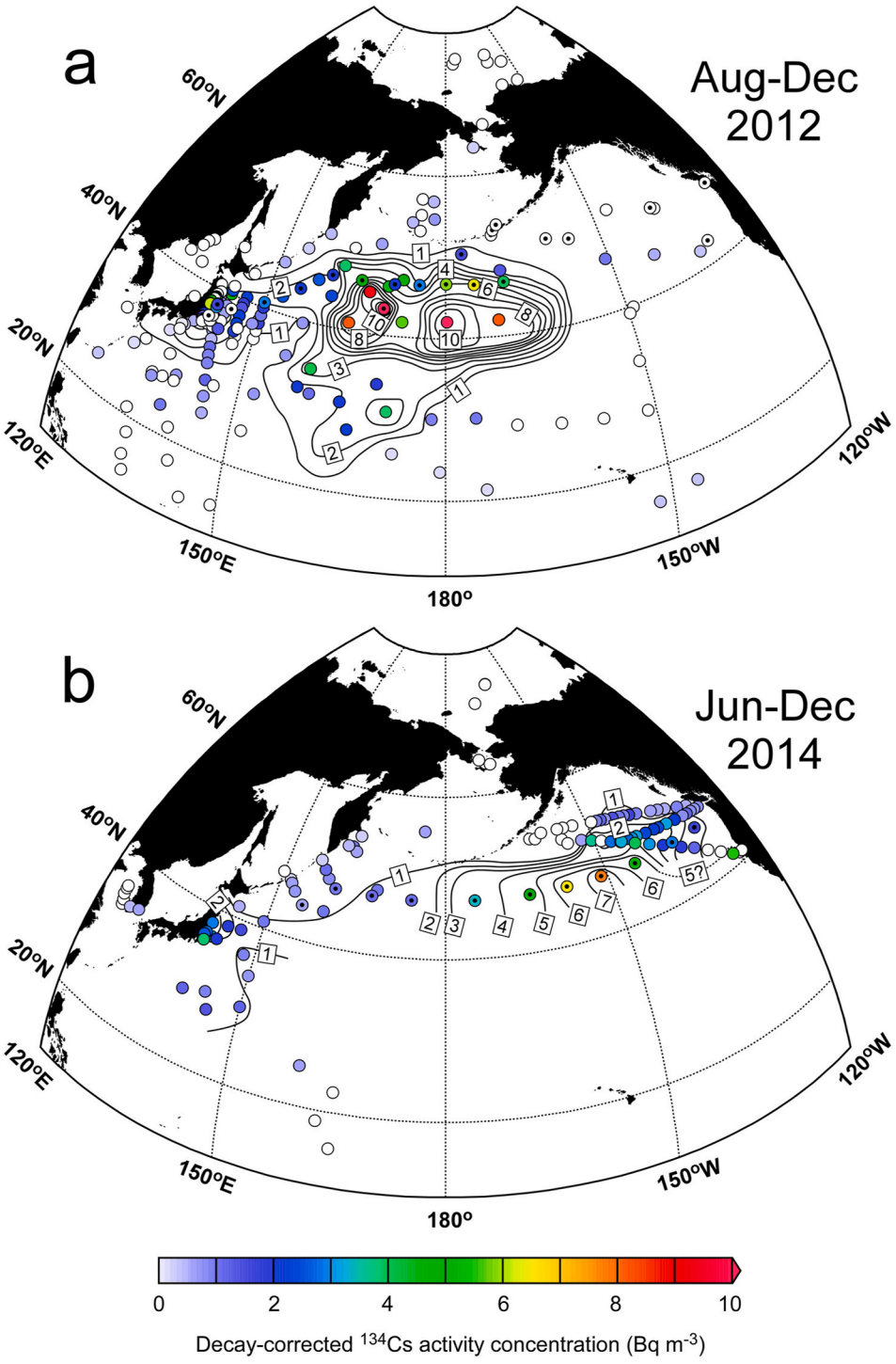

Fig. 4. (a) Activity concentrations of ^{134}Cs (Bq m^{-3}) in surface seawaters (from the sea surface to depth of 30 m) collected in the North Pacific Ocean and its marginal seas between August and December 2012. All data are decay-corrected to the accident date, 11 March 2011. Circles with a center dot indicate new data of this study from the KH-12-4 cruise. The contour interval is 1 Bq m^{-3}. (b) Same as (a) but for June to December 2014. Circles with a center dot indicate new data of this study from the MR14-04-Leg2 cruise.

available on the CCHDO web page (CCHDO, 2021).

3. Results and discussion

3.1. Surface concentrations in 2012 and 2014

First, to obtain an overview of the ^{134}Cs spreading, we delineated semi-synoptic distribution maps of ^{134}Cs at the sea surface in summer 2012 (Fig. 4a) and summer 2014 (Fig. 4b). Fig. 4a has been modified from the one published previously (Kumamoto et al., 2016) by incorporating new data from the KH-12-4 cruise. The plume of water with a high ^{134}Cs concentration of more than 4 Bq m^{-3} had been transported to the central North Pacific (38–48°N/160°E–170°W approximately) by summer 2012, about one and a half years after the accident (Fig. 4a). And higher concentrations more than 7 Bq m^{-3} were observed between 40°N and 45°N approximately. This high-^{134}Cs water plume was derived from both atmospheric deposition near the FNPP1 and direct discharge from the FNPP1 (the yellow and red shadows in Fig. 2a) and transported eastward along with the Kuroshio Extension and North Pacific Currents (Fig. 1). The ^{134}Cs concentrations measured in areas remote from the FNPP1, the Bering Sea, east of 150°W, and south of 20°N, are probably attributable only to atmospheric deposition (Kumamoto et al., 2016). About two years later, in summer 2014, ^{134}Cs activity concentrations higher than 4 Bq m^{-3} were observed at stations along 47°N between 170°W and 140°W approximately and the highest concentration (7.78 ± 0.83 Bq m^{-3}) was observed at 47°N/151°W (Fig. 4b). This suggests that the plume of high-^{134}Cs water observed in longitudes of 160°E–170°W approximately in summer 2012 (Fig. 4a) had been transported eastward to 170°W–140°W approximately by summer 2014 (Fig. 4b). The meridional distributions in the central and eastern North Pacific in summer 2014 are unknown due to the lack of data. However, the core of the high-^{134}Cs water plume probably lay around 41–43°N/151°W, as it was observed along 152°W in 2015 (Macdonald et al., 2020).

3.2. Vertical profiles in 2014

Fig. 5a shows the depth section of ^{134}Cs along the nominal 47°N zonal line in July–August 2014 (Fig. 3). The plume of water with a ^{134}Cs concentration of more than 4 Bq m^{-3} was observed between approximately 170°W and 140°W. ^{134}Cs remained only in the surface layer, shallower than approximately 200 m, which corresponds to the maximum depth of surface mixing in the western subarctic area in mid-winter (Ohno et al., 2009). At 151°W, where the highest concentration at the surface was found, the highest concentration (8.64 ± 0.70 Bq m^{-3}) was observed at 50 m depth. The activity concentration in the surface mixed-layer decreased in proportion to the distance from 151°W. This bell-shaped distribution suggests that the core of the high-^{134}Cs water plume, which was observed in the central North Pacific in summer 2012 (Fig. 4a), had not been completely eroded and reached around 151°W by summer 2014.

Fig. 5b shows the depth section along a northwest–southeast line

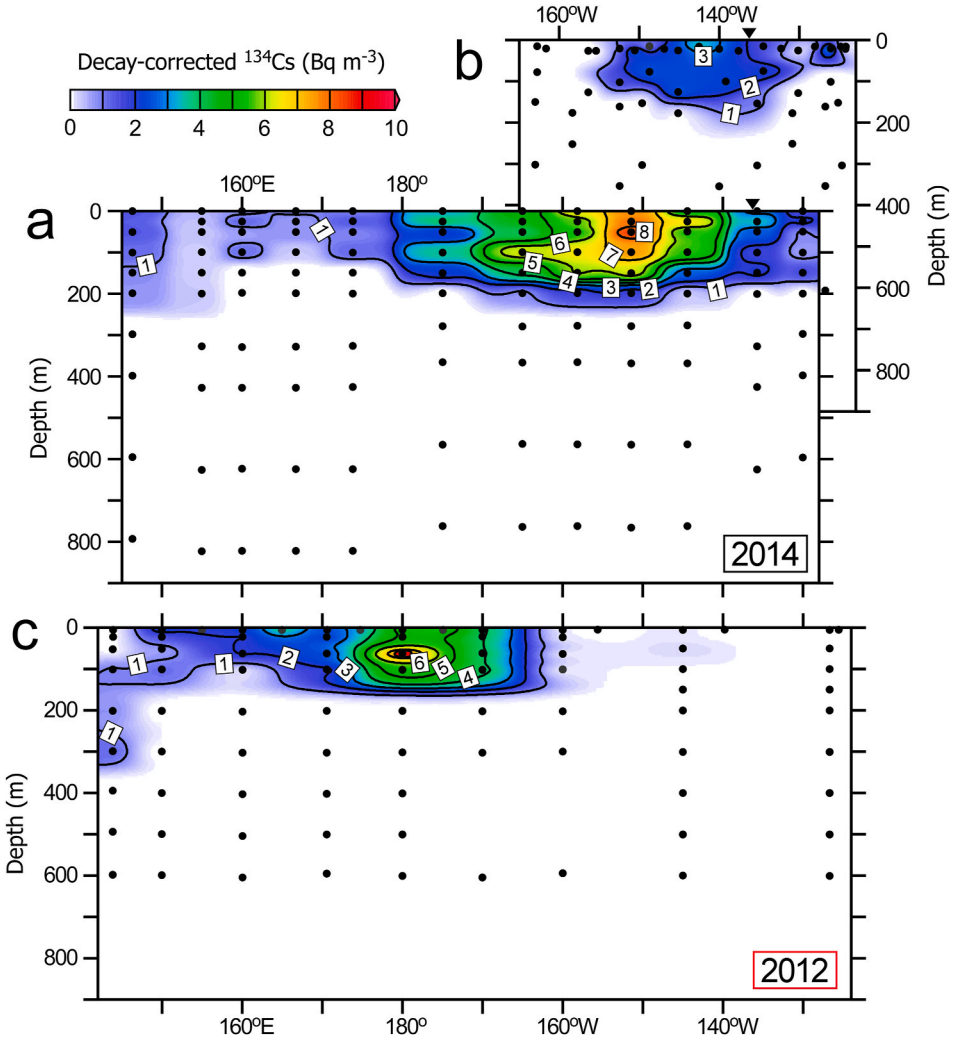

Fig. 5. (a) Depth section of ^{134}Cs (Bq m^{-3}) along the zonal line of the MR14-04-Leg2 cruise (Fig. 3) between July and August 2014. All data are decay-corrected to the accident date, 11 March 2011. Black dots show the sampling depths at each station. The contour interval is 1 Bq m^{-3}. (b) Same as (a), but along the zonal line of the Eureka cruise (Fig. 3) between July and August 2014 (Yoshida et al., 2015). (c) Same as (a), but along the zonal line of the KH-12-4 cruise and Line P (Fig. 3) between May and September 2012.

across the Gulf of Alaska, Eureka line (Fig. 3) in the same period, July–August 2014 (Yoshida et al., 2015). ^{134}Cs was also confined to the surface layer shallower than approximately 200 m. A plume of water with a ^{134}Cs concentration of more than 2 Bq m^{-3} was observed between approximately 150°W and 135°W. The distribution at the sea surface (Fig. 4b) indicates that the core of the high-^{134}Cs water plume had moved northeastward in the Gulf of Alaska along with the surface currents (Fig. 1). This northeastward transport in the Gulf of Alaska was also observed in summer 2015 (Smith et al., 2017). The surface distribution in the Gulf of Alaska (Fig. 4b) also suggests that the FNPP1-derived ^{134}Cs had been transported into the complex or eddy-rich region in which the California Current is forming.

3.3. Subsurface maxima in 2014

Along the 47°N line in 2014, we observed subsurface maxima at 25 and 100 m depths at stations east and west of 151°W, respectively (Fig. 5a). A similar deeper maximum was also observed at 47°N/152°W in June 2015 (Macdonald et al., 2020). Fig. 6a shows the sectional view of ^{134}Cs against seawater density anomaly (σ_θ) along the 47°N zonal line in July–August 2014. The deeper ^{134}Cs maximum in the west was in the subsurface layer with a potential density anomaly of around 26.1 kg m^{-3}

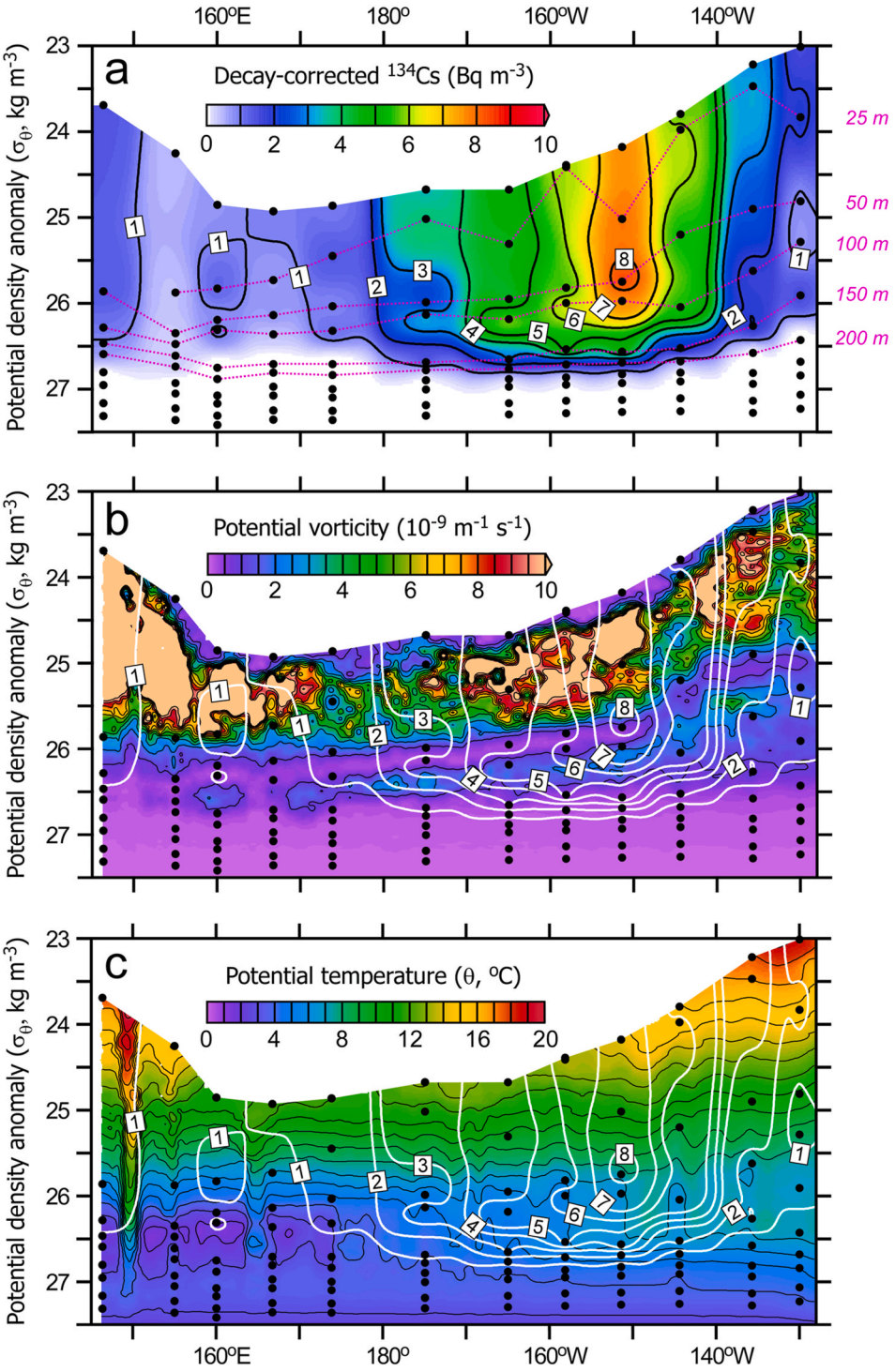

Fig. 6. (a) Water-density section of ^{134}Cs (Bq m^{-3}) along the zonal line of the MR14-04-Leg2 cruise (Fig. 3) between July and August 2014. The y-axis is the potential density anomaly (σ_θ, kg m^{-3}). All data are decay-corrected to the accident date, 11 March 2011. Black dots show the sampling depths at each station. The contour interval is 1 Bq m^{-3}. Dotted lines indicate the 25, 50, 100, 150, and 200 m iso-depths. (b) Same as (a), but showing potential vorticity (10^{-9} m^{-1} s^{-1}) in the background. The contour interval for potential vorticity is 0.5 × 10^{-9} m^{-1} s^{-1}. (c) Same as (a), but showing potential temperature (θ, °C) in the background. The contour interval for potential temperature is 1 °C.

σ_θ. The zonal section of potential vorticity (PV, Fig. 6b) shows that the deeper maximum of ^{134}Cs lay just under a subsurface PV minimum at around 26.0 kg m^{-3} σ_θ, which shoaled from west to east. PV (m^{-1} s^{-1}) calculated by the following equation is a quantity related to vorticity and seawater stratification.

$$PV = \frac{f}{g} N^2 \quad (1)$$

where f is the Coriolis parameter (s^{-1}), g is the gravitational acceleration (m s^{-2}), and N is the Brunt–Väisälä frequency (s^{-1}). In general, high and low PV values indicate the presence of a pycnocline and a pycnostad, respectively. As shown in Fig. 6b, the layers from the surface to about 800 m depth were the seasonal vertical mixed-layer (low PV), seasonal pycnocline (notably high PV), near bottom of mid-winter vertical mixed-layer (low PV), permanent pycnocline (high PV), and deep water (low PV).

Fig. 6c shows the zonal section of potential temperature. In the area west of 175°E, there was a water temperature minimum between approximately 26.3 and 26.6 kg m^{-3} σ_θ that corresponds to approximately 100–200 m depth. This temperature minimum was derived from mid-winter vertical mixing to about 200 m in the western subarctic gyre. As a result of this deep vertical mixing, the FNPP1-derived ^{134}Cs penetrated to about 200 m depth in the area offshore of the FNPP1 (145−155°E) in March 2011 (Kumamoto et al., 2014). During the eastward transport of this high-^{134}Cs water plume, it was eroded vertically by local mid-winter surface mixing, which was shallower than that in the area offshore of the FNPP1 (Fig. 6b). As a result, the high-^{134}Cs water below the local mid-winter mixed-layer depth remained and made a subsurface maximum. The formation processes of the shallow maximum (25 m depth) in the east are uncertain because of sparse observational data. However, the steep water density gradient at the sea surface in the area east of 151°W implies the eastward subduction of surface water with a higher concentration of ^{134}Cs into subsurface isopycnal layers between 23.5 and 24.0 kg m^{-3} σ_θ approximately.

3.4. Vertical profiles in 2012

Vertical profiles of ^{134}Cs from the KH-12-4 cruise have been already reported by Inomata et al. (2018), but they did not discuss their zonal distribution. In Fig. 5c, we drew a zonal section of ^{134}Cs by using data from the KH-12-4 cruise in August−September 2012 and the cruise in the Gulf of Alaska in May−June 2012 (Smith et al., 2015). Because the zonal lines west of 170°W in 2012 and 2014 overlapped (Fig. 3), we can directly compare the ^{134}Cs distribution west of 170°W in 2012 to that in 2014. The plume of water with a^{134}Cs concentration of more than 4 Bq m^{-3} was observed between approximately 180°W and 170°W in the surface layer shallower than 100 m depth. This high-^{134}Cs water plume was identified as a northern part of the water plume observed at the sea surface in the central North Pacific in August−December 2012 (Fig. 4a). The highest concentration (9.32 ± 0.44 Bq m^{-3}) was observed in the subsurface (62 m depth) at 180°W. This subsurface maximum also implied vertical erosion of the water plume in the shallower layer during the second winter (February–March 2012) after the FNPP1 accident as shown in the vertical profiles in 2014 (Fig. 5a). Although the maximum concentration at 180°W in 2012 is close to that observed at 151°W in 2014 (8.64 ± 0.70 Bq m^{-3}), the apparent zonal dimension of the high-^{134}Cs water plume along 47°N in 2012 (Fig. 5c) was smaller than that along 47°N in 2014 (Fig. 5a). This suggests a northward shift of the core of the water plume during its eastward transport along the surface currents (Fig. 1). If it is assumed that the core of the water plume was transported along 40°N from the FNPP1 (141°E) in April 2011 to 180°W in September 2012 and then from 180°W in September 2012 to 151°W in August 2014, the eastward transport speeds can be calculated as 7.0 cm s^{-1} and 3.8 cm s^{-1}, respectively. The slower transport speed in the east can be explained by a slowdown of the North Pacific Current (Fig. 1) in the eastern North Pacific (Aoyama et al., 2016b).

3.5. Penetration depth

The penetration depth of the high-^{134}Cs water plume along 47°N in 2014 (Fig. 5a) was apparently deeper than that observed in 2012 (Fig. 5c). The mean penetration depth (MPD, m), which is defined as the vertical inventory (Bq m^{-2}) divided by the activity concentration at the sea surface (Bq m^{-3}), can be used as an indicator to quantify the one-dimensional penetration of a chemical tracer from the sea surface into deep water. The vertical inventory of ^{134}Cs was determined by simple trapezoidal integration of activity concentrations versus depth (Table S4). The uncertainty of the vertical inventory was calculated from those of the concentrations at the sampling layers. The MPD at stations north of 44°N was calculated to be 170 ± 15 m in 2012 and 176 ± 8 m in 2014 (Fig. 7). This small temporal change in the MPD suggests that the penetration depth of ^{134}Cs did not deepen in the subarctic gyre between 2012 and 2014, an inference that is consistent with the conclusion that the shallower local vertical-mixing in the central and eastern areas than in the western area of the subarctic gyre did not deepen the penetration depth of the FNPP1-derived ^{134}Cs during its eastward transport.

3.6. Vertical inventory in 2014

The vertical inventories based on data of the MR14-04-L2 cruise in July−August 2014 are shown in Fig. 8. The highest vertical inventory (1420 ± 123 Bq m^{-2}) was observed at 151°W, where the highest activity concentration was also measured (Fig. 5a). The zonal distribution of the vertical inventory was symmetric around the maximum at 151°W. Fig. 8 also shows the vertical inventories based on data from the Eureka line in the same period, July−August 2014 (Yoshida et al., 2015). At the cross-point of the two cruise lines (46−47°N/136−135°W), the vertical inventory from the MR14-04-L2 cruise data (426 ± 66 Bq m^{-2}) was similar to that from the Eureka cruise data (349 ± 56 Bq m^{-2}). In the area west of the cross-point, the vertical inventory at the southern station (47°N/144°W) from the MR14-04-L2 cruise data (882 ± 99 Bq m^{-2}) was larger than that at the northern station (50°N/145°W) from the

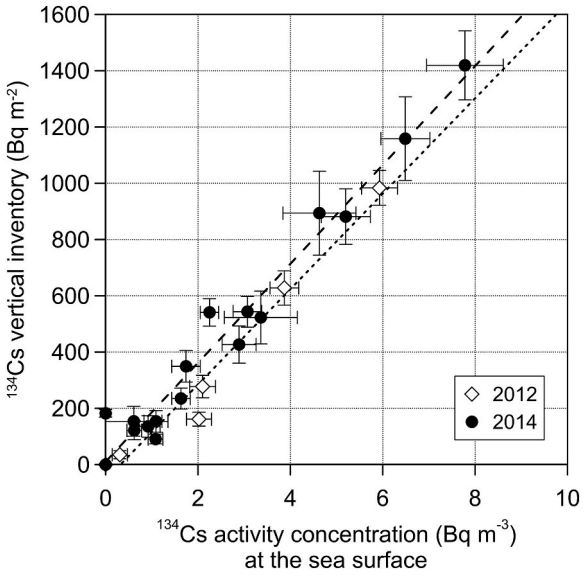

Fig. 7. Vertical inventory of ^{134}Cs (Bq m^{-2}) in relation to the activity concentration of ^{134}Cs at the sea surface (Bq m^{-3}) at stations north of 44°N in 2012 (diamonds) and 2014 (circles). All data were decay-corrected to the accident date, 11 March 2011. The dotted and dashed lines are linear regression lines fitted to the data in 2012 ($Y = 169.6 \times X - 54.5$, $r^2 = 0.9694$, $n = 6$) and in 2014 ($Y = 175.8 \times X + 10.4$, $r^2 = 0.9678$, $n = 18$), respectively. The slopes of these lines represent the mean penetration depth.

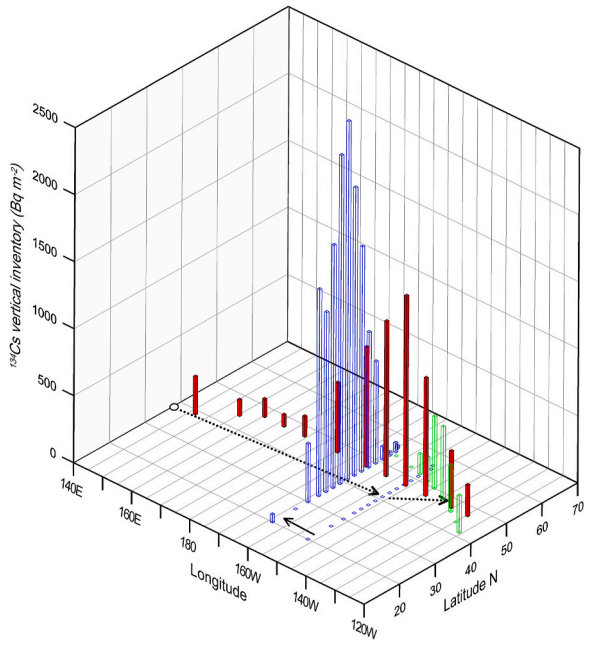

Fig. 8. Vertical inventories of ^{134}Cs (Bq m^{-2}). Red and green skeleton bars indicate data from the MR14-04-Leg2 and Eureka (Yoshida et al., 2015) cruises, respectively, in July–August 2014 (Fig. 3). Blue skeleton bars show data from the WOCE-P16N cruise in April–June 2015 (Macdonald et al., 2020). The WOCE-P16N meridional line along 152°W in 2015 was shifted to 164°W (solid line arrow), the estimated position in 2014 (see text). All data are decay-corrected to the accident date, 11 March 2011. The circle shows the location of the FNPP1. Dotted line arrows indicate the inferred transport directions of the core of the high-^{134}Cs water plume along surface currents. (For interpretation of the references to colour in this figure legend, the reader is referred to the Web version of this article.)

Eureka cruise data (541 ± 49 Bq m^{-2}). On the other hand, in the area east of the cross point, the vertical inventory at the southern station (44°N/130°W) from the Eureka cruise data (0 Bq m^{-2}) was smaller than that at the northern station (47°N/130°W) from the MR14-04-L2 cruise data (235 ± 37 Bq m^{-2}). These meridional gradients in the vertical inventory also suggested the northeastward shift of the core of the water plume in the Gulf of Alaska although we cannot confirm this shift in the area south of 47°N due to the lack of observational data (Fig. 4b).

3.7. Meridional distribution and inventory along152°W in 2015

It would be possible to estimate the three-dimensional size of the high-^{134}Cs water plume observed in 2014 if we had a simultaneous meridional distribution intersecting the zonal distribution along 47°N. Although we have no meridional observation in the North Pacific in 2014, the dataset of ^{134}Cs nominally along 152°W was obtained in June 2015 (Macdonald et al., 2020). Along 152°W, the plume of water with a^{134}Cs concentration of more than 4 Bq m^{-3} was observed in the surface layer shallower than about 300 m depth between approximately 32°N and 49°N. And the core of the water plume with concentrations higher than 7 Bq m^{-3} was found between 41°N and 43°N, which suggests that the core water slightly moved northward during its eastward transport from the FNPP1 (37.4°N/141.0°E) to the 152°W meridional line (Fig. 8). Combining the zonal distribution along 47°N in 2014 with the meridional distribution along 152°W in 2015, we simply estimated that the high-^{134}Cs water plume in the surface layer had extended from 32°N to 49°N latitude and from 170°W to 140°W longitude by August 2014 at least (Fig. 2b).

In June 2015, the highest vertical inventory of ^{134}Cs (2678 ± 189 Bq m^{-2}) along 152°W was observed at 41°N, and the vertical inventory distribution was symmetric around this highest value (Fig. 8). The vertical inventory at 47°N/152°W in June 2015 (1014 ± 126 Bq m^{-2}) was smaller than that at 47°N/151°W in August 2014 (1420 ± 123 Bq m^{-2}). If ^{134}Cs on the 152°W meridional line observed in June 2015 had been transported from the west at a constant speed of 3.8 cm s^{-1}, in August 2014 it would have been located approximately on the 164°W meridional line (Fig. 8). The vertical inventories at the hypothetical cross-point (47°N/165–164°W) in August 2014 of the zonal (894 ± 149 Bq m^{-2}) and meridional (1014 ± 126 Bq m^{-2}) lines agreed within their uncertainties (standard deviations). This agreement supports the assumption that the ^{134}Cs along the 152°W meridional line in June 2015 had been transported from the 164°W meridional line since August 2014.

3.8. Total inventory

The combination of the data from the two cruises along 47°N in 2014 and 152°W in 2015 also allowed us to estimate the total inventory of ^{134}Cs in the surface layer of the North Pacific. The meridionally integrated inventory (meridional inventory) along 152°W between 30°N and 51°N in 2015 was calculated to be (3.61 ± 0.37) × 10^{9} Bq m^{-1}. We assumed that the proportionality between this meridional inventory along 152°W and the vertical inventory at 47°N/152°W in 2015 was valid for the ^{134}Cs data obtained in 2014. By applying the proportionality coefficient to the vertical inventories (Bq m^{-2}) at stations between 160°E and 130°W along 47°N in 2014, we estimated the meridional inventory (Bq m^{-1}) along the meridional line at each station. Then, the total inventory (Bq) in the area between 30°N and 51°N latitude and between 160°E and 130°W longitude was calculated to be 13.4 ± 2.9 PBq from the zonal integration of the meridional inventories. Judging from the ^{134}Cs distribution at the sea surface in summer 2014 (Fig. 4b) and the distribution of the inventory (Fig. 8), the estimated total inventory included more than 95% of the observed ^{134}Cs in the North Pacific Ocean north of 30°N. It should be noted that this inventory in the subarctic North Pacific north of 30°N (the orange and light-yellow shadows in Fig. 2b) did not include ^{134}Cs in the subsurface STMW in the western subtropical gyre (the green shadow in Fig. 2b) and the surface layer in the eastern subtropical gyre, where there was no observational data.

The calculation of the total inventory is based on the assumption that the core of the high-^{134}Cs water plume lay around 41–43°N between 160°E and 130°W longitude. Fig. 8 indicates that this assumption was valid in the area west of 150°W approximately. On the other hand, in the area east of 150°W, the core of the water plume moved northeastward distinctly along with the surface currents (Fig. 1). As a result, the assumption was invalid in the area east of 150°W, where the meridional inventories were probably overestimated. We recalculated the meridional inventories along 144°W, 136°W, and 130°W lines in 2014 using revised proportionality coefficients between the meridional inventory along 152°W and the vertical inventories not at 47°N but 45°N, 43°N, and 41°N along 152°W in 2015, respectively. Finally, the total inventory in the subarctic North Pacific in August 2014 was corrected to 12.0 ± 2.4 PBq.

Macdonald et al. (2020) estimated the total inventory of the FNPP1-derived ^{134}Cs in the subarctic North Pacific to be 11–16 PBq only using the meridional distribution of ^{134}Cs along 152°W in 2015. The total inventory in 2014 estimated in this study is within this range but more robust because it is derived from the combining the meridional and zonal distributions. Inomata et al. (2018) also estimated the total inventory of ^{134}Cs in the subarctic North Pacific from the surface distribution (Fig. 4a) and the MPD in summer 2012 derived from the vertical profiles (Fig. 5c) to be 8.6 ± 1.5 PBq. This total inventory in 2012 is smaller than that in 2014 (12.0 ± 2.4 PBq), although they are supposed to be equivalent. We found that the total inventory in 2012 in Inomata et al. (2018) was underestimated by about 25%. The vertical inventory can be calculated by multiplying the surface concentration with the MPD. They, however, incorrectly assumed that the "surface

concentration" was constant from the surface to the middle of the MPD but decreased monotonically from the middle to the MPD. The corrected total inventory in 2012, 11.5 ± 2.0 PBq, agrees well with the total inventory in 2014 estimated in this study.

4. Conclusions

The previous studies (Aoyama et al., 2016b; Kaeriyama et al., 2013; Smith et al., 2017) revealed that the high-^{134}Cs water plume at the sea surface, which was originated from the atmospheric-deposited ^{134}C near the FNPP1 and directly-discharged ^{134}Cs from the FNPP1, had been transported across the subarctic gyre between Japan and the North American continent by 2016. In this study, we elucidated the vertical transport process of the high-^{134}Cs water plume during the eastward transport for the first time. ^{134}Cs had remained in the surface layer shallower than 200 m depth approximately until summer 2014. The MPD of ^{134}Cs (about 170–180 m) did not deepen from summer 2012 to summer 2014 because the local surface mixed-layer depth in the mid-winter shoaled from west to east. Subsequently, little eroded, the high-^{134}Cs water plume was transported westward along with the anti-clockwise subarctic gyre circulation (Fig. 1) and conveyed to the Bering Sea by 2017 (Huang et al., 2020; Inoue et al., 2020; Kumamoto et al., 2019). It is beyond the scope of this study to discuss quantitatively the vertical and horizontal water mixing in the subarctic gyre. However, the temporal change in the three-dimensional size of the high-^{134}Cs water plume (Fig. 2) could allow us to discuss the water mixing process in the subarctic gyre.

Combining the zonal distribution along 47°N in 2014 with the meridional distribution along 152°W in 2015, we elucidated the three-dimensional size of the high-^{134}Cs water plume in summer 2014 (the orange shadow in Fig. 2b). Also, using these data, we obtained the more robust inventory of ^{134}Cs in the subarctic North Pacific (12.0 ± 2.4 PBq) than those in the previous works (Inomata et al., 2018; Macdonald et al., 2020). The difference between the total input (15–20 PBq) and the inventory in the subarctic gyre (about 12 PBq) is 3–8 PBq, which agrees with the inventory in the subsurface STMW in the western subtropical gyre (3–6 PBq). This agreement is consistent with the small inventory in the eastern subtropical gyre that is suggested by the meridional observation along 152°W in 2015 (Macdonald et al., 2020). However, the southward transport into the subtropical gyre along with the subduction of CMW has not been observed yet (the blue arrow in Fig. 2b). Thus, at present, the inventory in the subtropical North Pacific is still unknown. New observational data from zonal and meridional cross-sections in the subtropical gyre similar to those in this study will allow us to estimate a more robust inventory of the FNPP1-derived ^{134}Cs in the subtropical gyre and then the whole (subarctic + subtropical) North Pacific Ocean.

Declaration of competing interest

The authors declare that they have no known competing financial interests or personal relationships that could have appeared to influence.

Acknowledgments

We would like to thank Dr. John N. Smith for sharing data in the Gulf of Alaska in 2014 and for his valuable comments. This work was partially supported by a Grant-in-Aid for Scientific Research on Innovative Areas from Ministry of Education, Culture, Sports, Science and Technology of Japan (KAKENHI), #24110004. Figs. 1–6 were drawn using Ocean Data View software (Schlitzer, 2021).

Appendix A. Supplementary data

Supplementary data to this article can be found online at https://doi.org/10.1016/j.jenvrad.2022.106864.

References

Aoyama, M., Hamajima, Y., Hult, M., Uematsu, M., Oka, E., Tsumune, D., Kumamoto, Y., 2016b. ^{134}Cs and ^{137}Cs in the north Pacific Ocean derived from the March 2011 TEPCO Fukushima dai-ichi nuclear power plant accident, Japan. Part one: surface pathway and vertical distributions. J. Oceanogr. 72, 53–65.

Aoyama, M., Hamajima, Y., Inomata, Y., Oka, E., 2017. Recirculation of FNPP1-derived radiocaesium observed in winter 2015/2016 in coastal regions of Japan. Appl. Radiat. Isot. 126, 83–87.

Aoyama, M., Hirose, K., 2008. Radiometric determination of anthropogenic radionuclides in seawater. In: Povinec, P.P. (Ed.), Analysis of Environmental Radionuclides, Radioactivity in the Environment, vol. 2. Elsevier, Amsterdam, London, pp. 137–162.

Aoyama, M., Kajino, M., Tanaka, T.Y., Sekiyama, T.T., Tsumune, D., Tsubono, T., Hamajima, Y., Inomata, Y., Gamo, T., 2016a. ^{134}Cs and ^{137}Cs in the north Pacific Ocean derived from the March 2011 TEPCO Fukushima dai-ichi nuclear power plant accident, Japan. Part two: estimation of ^{134}Cs and ^{137}Cs inventories in the north Pacific Ocean. J. Oceanogr. 72, 67–76.

Aoyama, M., Uematsu, M., Tsumune, D., Hamajima, Y., 2013. Surface pathway of radioactive plume of TEPCO Fukushima NPP1 released ^{134}Cs and ^{137}Cs. Biogeosciences 10, 3067–3078.

Buesseler, K., Aoyama, M., Fukasawa, M., 2011. Impacts of the Fukushima nuclear power plants on marine radioactivity. Environ. Sci. Technol. 45, 9931–9935.

Buesseler, K., Dai, M., Aoyama, M., Benitez-Nelson, C., Charmasson, S., Higley, K., Maderich, V., Masqué, P., Morris, P.J., Oughton, D., Smith, J.N., 2017. Fukushima Daiichi–derived radionuclides in the ocean: transport, fate, and impacts. Ann. Rev. Mar. Sci 9, 173–203.

CCHDO, 2021. CLIVAR (Climate Variability and Predictability) & Carbon Hydrographic Data Office. CCHDO. https://cchdo.ucsd.edu/. (Accessed 20 December 2021).

Huang, D., Lin, J., Du, J., Yu, T., 2020. The detection of Fukushima-derived radiocesium in the Bering Sea and Arctic Ocean six years after the nuclear accident. Environ. Pollut. 256, 113386.

Inomata, Y., Aoyama, M., Tsubono, T., Tsumune, D., Kumamoto, Y., Nagai, H., Yamagata, T., Kajino, M., Tanaka, Y.T., Sekiyama, T.T., Oka, E., Yamada, M., 2018. Estimate of fukushima-derived radiocaesium in the north Pacific Ocean in summer 2012. J. Radioanal. Nucl. Chem. 318, 1587–1596.

Inoue, M., Shirotani, Y., Nagao, S., Aramaki, T., Kim, Y.I., Hayakawa, K., 2018. Spatial variations of ^{226}Ra, ^{228}Ra, ^{134}Cs, and ^{137}Cs concentrations in western and southern waters off the Korean Peninsula in July 2014. J. Environ. Radioact. 182, 151–156.

Inoue, M., Shirotani, Y., Nagao, S., Kofuji, H., Volkov, Y.N., Nishioka, J., 2016. Migration of the FDNPP-derived ^{134}Cs and ^{137}Cs along with ^{226}Ra and ^{228}Ra concentrations across the northwestern North Pacific ocean. J. Environ. Radioact. 162–163, 33–38.

Inoue, M., Takehara, R., Hanaki, S., Kameyama, H., Nishioka, J., Nagao, S., 2020. Distributions of radiocesium and radium isotopes in the western Bering Sea in 2018. Mar. Chem. 225, 103843.

Japan Nuclear Regulation Authority (JNRA), 2021. Readings of Sea Area Monitoring. http://radioactivity.nsr.go.jp/en/list/205/list-1.html. (Accessed 20 December 2021).

Kaeriyama, H., Ambe, D., Shimizu, Y., Fujimoto, K., Ono, T., Yonezaki, S., Kato, Y., Matsunaga, H., Minami, H., Nakatsuka, S., Watanabe, T., 2013. Direct observation of ^{134}Cs and ^{137}Cs in surface seawater in the western and central North Pacific after the Fukushima Dai-ichi nuclear power plant accident. Biogeosciences 10, 4287–4295.

Kaeriyama, H., Shimizu, Y., Ambe, D., Masujima, M., Shigenobu, Y., Fujimoto, K., Ono, T., Nishiuchi, K., Taneda, T., Kurogi, H., Setou, T., Sugisaki, H., Ichikawa, T., Hidaka, K., Hiroe, Y., Kusaka, A., Kodama, T., Kuriyama, M., Morita, H., Nakata, K., Morinaga, K., Morita, T., Watanabe, T., 2014. Southwest intrusion of ^{134}Cs and ^{137}Cs derived from the Fukushima dai-ichi nuclear power plant accident in the western North pacific. Environ. Sci. Technol. 48, 3120–3127.

Kaeriyama, H., Shimizu, Y., Setou, T., Kumamoto, Y., Okazaki, M., Ambe, D., Ono, T., 2016. Intrusion of Fukushima-derived radiocaesium into subsurface water due to formation of mode waters in the North Pacific. Sci. Rep. 6, 22010.

Kumamoto, Y., Aoyama, M., Hamajima, Y., Aono, T., Kouketsu, S., Murata, A., Kawano, T., 2014. Southward spreading of the fukushima-derived radiocesium across the Kuroshio extension in the north pacific. Sci. Rep. 4, 4276.

Kumamoto, Y., Aoyama, M., Hamajima, Murata, A., Kawano, T., 2015. Impact of Fukushima-derived radiocesium in the western North Pacific Ocean about ten months after the Fukushima Dai-ichi nuclear power plant accident. J. Environ. Radioact. 140, 114–122.

Kumamoto, Y., Aoyama, M., Hamajima, Y., Nagai, H., Yamagata, T., Kawai, Y., Oka, E., Yamaguchi, A., Imai, K., Murata, A., 2017a. Fukushima-derived radiocesium in the western North pacific in 2014. J. Radioanal. Nucl. Chem. 311, 1209–1217.

Kumamoto, Y., Aoyama, M., Hamajima, Y., Nishino, S., Murata, A., Kikuchi, T., 2016. Meridional distribution of Fukushima-derived radiocesium in surface seawater along a trans-Pacific line from the Arctic to Antarctic Oceans in summer 2012. J. Radioanal. Nucl. Chem. 307, 1703–1710.

Kumamoto, Y., Aoyama, M., Hamajima, Y., Nishino, S., Murata, A., Kikuchi, T., 2017b. Radiocesium in the western subarctic area of the north Pacific Ocean, Bering Sea, and arctic ocean in 2013 and 2014. Appl. Radiat. Isot. 126, 88–92.

Kumamoto, Y., Aoyama, M., Hamajima, Y., Nishino, S., Murata, A., Kikuchi, T., 2019. Radiocesium in the western subarctic area of the north Pacific Ocean, Bering Sea, and arctic ocean in 2015 and 2017. Polar Science 21, 228–232.

Macdonald, A.M., Yoshida, S., Pike, S.M., Buesseler, K.O., Rypina, I.I., Jayne, S.R., Rossi, V., Kenyon, J., Drysdale, J.A., 2020. Fukushima tracer perspective on four years of North Pacific mode water evolution. Deep-Sea Res. I 166, 103379.

Masuzawa, J., 1969. Subtropical mode water. Deep-Sea Res. 16, 463–472.

Morino, Y., Ohara, T., Watanabe, M., Hayashi, S., Nishizawa, M., 2013. Episode analysis of deposition of radiocesium from the Fukushima daiichi nuclear power plant accident. Environ. Sci. Technol. 47, 2314–2322.

Ohno, Y., Iwasaka, N., Kobashi, F., Sato, Y., 2009. Mixed layer depth climatology of the North Pacific based on Argo observations. J. Oceanogr. 65, 1–16.

Oka, E., Qiu, B., 2012. Progress of North Pacific mode water research in the past decade. J. Oceanogr. 68, 5–20.

Pham, M.K., Betti, M., Povinec, P.P., Benmansour, M., Bünger, V., Drefvelin, J., Engeler, C., Flemal, J.M., Gascó, C., Guillevic, J., Gurriaran, R., Groening, M., Happel, J.D., Herrmann, J., Klemola, S., Kloster, M., Kanisch, G., Leonard, K., Long, S., Nielsen, S., Oh, J.-S., Rieth, P.U., Östergren, I., Pettersson, H., Pinhao, N., Pujol, L., Sato, K., Schikowski, J., Varga, Z., Vartti, V.P., Zheng, J., 2011. A certified reference material for radionuclides in the water sample from Irish Sea (IAEA-443). J. Radioanal. Nucl. Chem. 288, 603–611.

Rossi, V., Van Sebille, E., Sen Gupta, A., Garcon, V., England, M.H., 2013. Multi-decadal projections of surface and interior pathways of the Fukushima cesium-137 radioactive plume. Deep-Sea Res. I 80, 37–46.

Rypina, I.I., Jayne, S.R., Yoshida, S., Macdonald, A.M., Buesseler, K.O., 2014. Drifter-based estimate of the 5 year dispersal of Fukushima-derived radionuclides. J. Geophys. Res. Oceans 119, 8177–8193.

Schlitzer, R., 2021. Ocean Data View. https://odv.awi.de/. (Accessed 20 December 2021).

Smith, J.N., Brown, R.M., Williams, W.J., Robert, M., Nelson, R.N., Moran, S.B., 2015. Arrival of the Fukushima radioactivity plume in North American continental waters. Proc. Natl. Acad. Sci. U.S.A. 112, 1310–1315.

Smith, J.N., Rossi, V., Buesseler, K.O., Cullen, J.T., Cornett, J., Nelson, R., Macdonald, A. M., Robert, M., Kellogg, J., 2017. Recent transport history of Fukushima radioactivity in the northeast Pacific Ocean. Environ. Sci. Technol. 51, 10494–10502.

Suga, T., Takei, Y., Hanawa, K., 1997. Thermostad distribution in the North Pacific subtropical gyre: the central mode water and the subtropical mode water. J. Phys. Oceanogr. 27, 140–152.

Tsubono, T., Misumi, K., Tsumune, D., Bryan, F.O., Hirose, K., Aoyama, M., 2016. Evaluation of radioactive cesium impact from atmospheric deposition and direct release fluxes into the North Pacific from the Fukushima Daiichi nuclear power plant. Deep-Sea Res. I 115, 10–21.

Tsumune, D., Tsubono, T., Aoyama, M., Uematsu, M., Misumi, K., Maeda, Y., Yoshida, Y., Hayami, H., 2013. One-year, regional-scale simulation of ^{137}Cs radioactivity in the ocean following the Fukushima Dai-ichi Nuclear Power Plant accident. Biogeosciences 10, 5601–5617.

Yoshida, S., Macdonald, A.M., Jayne, S.R., Rypina, I.R., Buesseler, K.O., 2015. Observed eastward progression of the Fukushima ^{134}Cs signal across the north pacific. Geophys. Res. Lett. 42, 7139–7147.